Available online at www.sciencedirect.com
ScienceDirect
Magnetic Resonance Imaging 25 (2007) 1079–1088
MAGNETIC RESONANCE IMAGING

COmplex-Model-Based Estimation of thermal noise for fMRI data in the presence of artifacts

Yin Xu[a], Gaohong Wu[a], Daniel B. Rowe[a], Yuan Ma[a,b], Rongyan Zhang[a], Guofan Xu[a], Shi-Jiang Li[a,*]

[a]*Department of Biophysics, Medical College of Wisconsin, Milwaukee, WI 53226, USA*
[b]*GE Healthcare, Milwaukee, WI 53226, USA*

Received 21 November 2006; accepted 17 December 2006

Abstract

Due to the presence of artifacts induced by fast-imaging acquisition in functional magnetic resonance imaging (fMRI) studies, it is very difficult to estimate the variance of thermal noise by traditional methods in magnitude images. Moreover, the existence of incidental phase fluctuations impairs the validity of currently available solutions based on complex datasets. In this article, a time-domain model is proposed to generalize the analysis of complex datasets for nonbrain regions by incorporating artifacts and phase fluctuations. Based on this model, a novel estimation schema has been developed to find an appropriate set of voxels in nonbrain regions according to their levels of artifact and phase fluctuation. In addition, noise intensity from these voxels is estimated. The whole schema is named COmplex-Model-Based Estimation (COMBE). Theoretical and experimental results demonstrate that the proposed COMBE method provides a better estimation of thermal noise in fMRI studies compared with previously proposed methods and suggest that the new method can adapt to a broader range of applications, such as functional connectivity studies, evaluation of sequence designs and reconstruction schemas.

Keywords: Thermal noise; Complex-valued model; COmplex-Model-Based Estimation; fMRI; Human brain

1. Introduction

Thermal noise in magnetic resonance (MR) images is a very important parameter. The estimation of thermal noise not only provides measurements of the quality of a magnetic resonance imaging (MRI) system [1] and quantification of an MR signal, especially signal-to-noise ratio (SNR) for functional MRI (fMRI) signal [2], but also offers a general measure to evaluate the performance of MRI sequences [3] and reconstruction schemas [4].

Analytical estimation methods that determine thermal noise have been extensively studied. In most cases, thermal noise is determined from magnitude images, which can be modeled as a Rician distribution that has no analytical solution. When the SNR is high, the Rician distribution can be approximated as Gaussian in nature, and thermal noise can be estimated as the standard deviation of magnitude [5]. When the signal is zero, the Rician model evolves to a Rayleigh distribution, and thermal noise can be estimated by dividing the standard deviation of magnitude with a correctional factor (about 0.655) [6,7].

Technological development and clinical research applications of fMRI methods have generated three new challenges in estimating noise. First, unlike anatomical images, fMRI datasets in high SNR regions, such as the brain, contain significant temporal signal changes, hence invalidating the Gaussian method. Temporal signal changes may include fluctuations in blood-oxygenation-level-dependent (BOLD) signals induced by tasks or physiologic noise during rest [8]. Second, the presence of significant artifacts in background regions (nonbrain regions), acquired by fast-imaging methods such as Echo Planar Imaging (EPI) [9] and spiral [10] pulse sequences, makes the Rayleigh method inapplicable. To solve this problem, researchers have developed several methods, including averaging variances over real and imaginary channels (Average method) [11–13], maximum likelihood (ML)-based estimations [12,14] and a double-acquisition method employing the analytical form of even moments of the Rician distribution [15].

* Corresponding author. Tel.: +1 414 456 4029; fax: +1 414 456 6512.
E-mail address: sjli@mcw.edu (S.-J. Li).

0730-725X/$ – see front matter © 2007 Elsevier Inc. All rights reserved.
doi:10.1016/j.mri.2006.12.007

The final problem seen in fMRI datasets is incidental phase fluctuations, which are derived from various time-dependent sources of variation, including flip-angle inhomogeneity, filter responses, system delay, noncentered sampling windows and others [16]. However, the above-mentioned methods did not explicitly take phase fluctuation into account as a random variable.

In this article, a new method is proposed for fMRI datasets. It estimates thermal noise in the presence of image artifacts and phase fluctuations for fMRI datasets. By analyzing the real and imaginary channels of complex-valued data in the time domain, it becomes evident that thermal noise can be accurately estimated. Theoretical simulations and experimental results demonstrate that the new method, compared with previously proposed methods, provides a better estimation of thermal noise and a higher capacity for a broader range of artifact-to-noise ratios (ANRs) and phase fluctuations. Thus, the new method is suitable for various applications, including functional connectivity studies, sequence evaluation and reconstruction evaluation.

2. Theory

It is well known that in the brain, real $[R_b(t)]$ and imaginary $[I_b(t)]$ channels in a given voxel of reconstructed fMRI datasets have three components. These components are: the magnitude of the signal $S(t)$, the phase of the signal $\theta(t)$ and the thermal noise $n(t)$ at time t. The time-domain model within a given voxel can be expressed as:

$$R_b(t) = S(t)\cos(\theta(t)) + n_1(t)$$

$$I_b(t) = S(t)\sin(\theta(t)) + n_2(t) \quad (1)$$

where $n_1(t)$ and $n_2(t)$ are additive thermal measurement noise [17,18]. As previously described, the magnitude and phase portions of the signal are temporally varying quantities. Thus, they may be modeled by temporally constant mean-varying and time-varying portions $S(t)=S+\Delta S(t)$ and $\theta(t)=\theta+\Delta\theta(t)$. The temporally constant means of magnitude and phase are S and θ, while their time-varying portions are $\Delta S(t)$ and $\Delta\theta(t)$, respectively.

Any signal that is present in the background region of reconstructed fMRI datasets is due to ghosting artifacts. Thus, it is described by a decreased version of the original signal. The original magnitude signal $S(t)$ in Eq. (1) is decreased by an artifact proportionality factor γ to yield $\gamma S(t)=\gamma S+\gamma\Delta S(t)$ instead of $S(t)$ for an artifact-to-noise model.

In fMRI data, the mean magnitude signal is usually much larger than its temporal variation $S \gg \Delta S(t)$, so that the artifact magnitude signal is also much larger than its temporal variation $\gamma S \gg \gamma\Delta S(t)$. This allows the variation of the artifact signal to be neglected when $\gamma S(t)$ is comparable to thermal noise. Thus, the artifact $\gamma S(t)$ can be taken as a temporally constant quantity a, which is called the artifact level. The artifact-to-noise complex model can be written as:

$$R(t) = a\cos(\theta + \Delta\theta(t)) + n_1(t)$$

$$I(t) = a\sin(\theta + \Delta\theta(t)) + n_2(t). \quad (2)$$

In nonartifact voxels, $a=0$, so that real and imaginary channels consist only of noise. The phase fluctuation $\Delta\theta(t)$ in fMRI data is relatively small. This allows Eq. (2) to be written as:

$$R(t) = a\cos(\theta(t)) + n_1(t) \approx a(\cos\theta - \sin\theta\cdot\Delta\theta(t)) + n_1(t)$$

$$I(t) = a\sin(\theta(t)) + n_2(t) \approx a(\sin\theta + \cos\theta\cdot\Delta\theta(t)) + n_2(t) \quad (3)$$

with the use of trigonometric addition formulas for sines and cosines along with small-angle approximations.

By definition, thermal noise $n_1(t)$ and $n_2(t)$ in the two channels are mutually independent and identically distributed with zero means and variances σ_0^2. Additionally, the mean and the variance of phase fluctuation are zero and σ_θ^2, respectively. With the above model specifications, the mean (expected) values for the real and imaginary parts of the artifact-to-noise complex model are:

$$\mu_R = a\cos\theta$$

$$\mu_I = a\sin\theta \quad (4)$$

while their variances are:

$$\sigma_R^2 = a^2\sin^2\theta\cdot\sigma_\theta^2 + \sigma_0^2$$

$$\sigma_I^2 = a^2\cos^2\theta\cdot\sigma_\theta^2 + \sigma_0^2. \quad (5)$$

Since we do not assume any particular distribution for thermal noise and phase fluctuations, we do not have a likelihood and cannot estimate model parameters with maximum likelihood estimates (MLEs). Instead, we will estimate model parameters with method of moment estimators (MMEs). MMEs are found by equating population moments to sample moments [19]. MMEs for the artifact level a and the mean phase θ are found by equating population means to sample means (first moments). This yields the equations:

$$\overline{R} = \hat{a}\cos(\hat{\theta}); \quad \overline{I} = \hat{a}\sin(\hat{\theta}) \quad (6)$$

where $\bar{R}$ and $\bar{I}$ are the sample means of real and imaginary channels. The solution to these two equations with two unknowns yields MMEs that are:

$$\hat{a} = \sqrt{(\overline{R})^2 + (\overline{I})^2}; \quad \hat{\theta} = \tan^{-1}(\overline{I}/\overline{R}). \quad (7)$$

For convenience, $\hat{a}$ is named the artifact level, while $\hat{\theta}$ is the estimated phase mean. MMEs for variances σ_0^2 and σ_θ^2

can be found by equating population second moments to sample second moments. This yields the equations:

$$\hat{\sigma}_R^2 = \overline{R^2} - (\overline{R})^2 = \hat{\alpha}^2 \sin^2\hat{\theta}\cdot\hat{\sigma}_\theta^2 + \hat{\sigma}_0^2$$

$$\hat{\sigma}_I^2 = \overline{I^2} - (\overline{I})^2 = \hat{\alpha}^2 \cos^2\hat{\theta}\cdot\hat{\sigma}_\theta^2 + \hat{\sigma}_0^2 \tag{8}$$

where $\overline{R^2}$ and $\overline{I^2}$ are the means of the squares of the real and imaginary channels, respectively, while $\bar{R}$ and $\bar{I}$ remain as previously defined. The solution to these two equations with the two unknowns yields the following MMEs:

$$\hat{\sigma}_\theta^2 = \frac{\hat{\sigma}_I^2 - \hat{\sigma}_R^2}{\hat{\alpha}^2\cos(2\hat{\theta})}$$

$$\hat{\sigma}_0^2 = \frac{1}{2}\left(\hat{\sigma}_R^2 + \hat{\sigma}_I^2\right) - \frac{1}{2}\hat{\alpha}^2\hat{\sigma}_\theta^2. \tag{9}$$

It is noted that, in Eq. (9), the denominator for the estimate of the sample variance for phase fluctuation will approach zero when the estimated phase mean $\hat{\theta}$ is close to $(\pi/4)\cdot(2k-1)$, where k is any integer. To avoid this problem, a complementary set of equations is introduced:

$$\hat{\sigma}_{R+I}^2 = \overline{(R+I)^2} - \left(\overline{R+I}\right)^2 = \hat{\alpha}^2\hat{\sigma}_\theta^2\left(1-\sin(2\theta)\right) + 2\hat{\sigma}_0^2$$

$$\hat{\sigma}_{R-I}^2 = \overline{(R-I)^2} - \left(\overline{R-I}\right)^2 = \hat{\alpha}^2\hat{\sigma}_\theta^2\left(1+\sin(2\theta)\right) + 2\hat{\sigma}_0^2 \tag{10}$$

The terms $\hat{\sigma}_{R+I}^2$ and $\hat{\sigma}_{R+I}^2$ represent the estimated variance of the sum of channels and the difference between channels, respectively. Then, the sample variance for phase fluctuation can be obtained as below:

$$\hat{\sigma}_\theta^2 = \frac{\hat{\sigma}_{R-I}^2 - \hat{\sigma}_{R+I}^2}{2\hat{\alpha}^2\sin 2\theta}. \tag{11}$$

For convenience, this model will be parameterized by an ANR that is defined as $\eta = \hat{a}/\hat{\sigma}_0$. This proposed method is named COmplex-Model-Based Estimation (COMBE).

For evaluation, the four previously proposed noise-estimation methods (Gaussian, Rayleigh, Average and Simplex) are implemented for comparison through the theoretical simulation and experimental determination of the estimated noise level. In the case of the Gaussian method, the artifact level can be estimated in the usual way as the sample mean of the magnitude time course $\hat{a}_G = \overline{M}$, where $M(t) = \sqrt{(R(t))^2 + (I(t))^2}$ denotes magnitude at time t. Noise level can also be estimated from voxel magnitude time courses as:

$$\hat{\sigma}_{0G}^2 = \frac{1}{n-1}\sum_{t=1}^{n}(M(t) - \overline{M})^2. \tag{12}$$

In this study, we implement this method, which is from the background region, in order to obtain a reference demonstrating how the ANR affects estimation.

For the Rayleigh method, the artifact level can be estimated by $\hat{a}_R = \sqrt{\frac{2}{\pi}\hat{\sigma}_{0G}^2}$. Noise estimation is conducted by dividing the noise variance obtained from the Gaussian method with a constant factor as:

$$\hat{\sigma}_{0R}^2 = \frac{\hat{\sigma}_{0G}^2}{2-\pi/2} \tag{13}$$

as has been described previously [7]. The standard deviation of the noise is generally utilized. The widely used Rayleigh method selects voxels from background regions and assumes that these voxels contain only thermal noise without signals such as artifacts [17,20].

In the case of the Average method, the estimate of the artifact $\hat{a}_A$ is the same as our COMBE estimate. The estimate of noise variance is the average of the variances of real and imaginary datasets:

$$\hat{\sigma}_{0A}^2 = \frac{1}{2}\left(\hat{\sigma}_R^2 + \hat{\sigma}_I^2\right). \tag{14}$$

The Average method was utilized in voxel measurements in space [8], assuming a region of constant amplitude and phase. This method was also used through time [14] in a model developed for fMRI, which has a temporally varying magnitude signal with a linear form and a temporally constant phase. We use the Average method that was developed for fMRI with a specification of a temporally constant magnitude since we have repeated measurements. This yields the same estimates as the version used in space, but we do not assume spatial homogeneity.

Although the Average method takes into account the existence of the artifact, it could produce a biased estimation when phase fluctuations exist. Our model explicitly assumes, mirrors and estimates phase fluctuation, while the previous models do not. It should be noted that our COMBE MMEs for the mean artifact and phase are the same as the MLEs from the Average method. Furthermore, in comparing noise variance estimates in Eq. (9) to those in Eq. (14), the actual noise estimate by our COMBE method is:

$$\sigma_0^2 = \hat{\sigma}_{0A}^2 - a^2\sigma_\theta^2/2. \tag{15}$$

Our COMBE MME for noise variance is the same as the MLE from the Average method when there is no phase fluctuation. This demonstrates that our model is more general in nature and that, when phase fluctuations do not exist, our COMBE method produces an identical estimate of noise variance as the Average method. However, when phase fluctuations exist, the two methods deviate from our estimate. Noise variances become decreased, accounting for the additional phase variation that we have modeled and estimated.

The Simplex method has a noise level that can be estimated based on the magnitude image by maximizing a

two-dimensional function following the description by Sijbers and den Dekker [12] (Eq. (46) in the cited article). Although Rician function cannot be analytically solved, numerical optimization can be implemented by using the Nelder–Mead Simplex method [21].

3. Simulations and results

A simulated data study was conducted in order to examine the theoretical properties of our COMBE model in comparison to the other previously described models under known conditions. Real $R(t)$ and imaginary $I(t)$ voxel time courses were generated according to the COMBE model in Eq. (3). This similarity to experimental data will be presented in Section 4. From these simulations, we can examine the impact of ANR level and phase fluctuation standard deviation on the estimation of noise intensity under known conditions.

In statistical analysis, desirable properties of parameter estimates are unbiased (correct on average) and have the smallest standard deviation (on average). The smallest standard deviations that are unbiased are generally determined using the expected value and the Cramer–Rao lower bound for the variance of an estimator from a model resulting in likelihood. However, since we do not make any distributional assumptions, we evaluate these properties via Monte Carlo simulation.

For our simulation, we utilized MATLAB to generate voxel time courses that are of the length of 100 in order to mimic the experimental data that will be presented in Section 4. The voxels were generated in an array where each element has a different ANR and thermal noise standard deviation. The phase mean θ for each voxel was randomly chosen by using a uniformly distributed random function from 0 to 2π rad, while the thermal noise standard deviation σ_0 was generated with channel-independent white Gaussian (normally)-distributed noise with a mean of zero and a variance of one. The ANR varied from zero to five from left to right along the horizontal direction. Phase fluctuation was generated with a mean of zero and a standard deviation σ_θ that varied from 0 to $\pi/2$ rad from bottom to top. Both ANR and phase fluctuation varied in 101 equally spaced increments. This procedure was repeated for 100 arrays of voxel time courses. The parameters for each of the models were estimated within each of the arrays. Array surfaces for the sample mean and mean square error (MSE) of the estimated standard deviation of thermal noise by each method were computed as a function of the ANR and σ_θ^2.

The joint dependence of the thermal noise standard deviation as a function of the ANR and the phase fluctuation standard deviation are presented as matrix maps in Fig. 1 with a color bar in Fig. 1F, while matrix maps for MSEs are omitted here. The true noise standard deviation in the figure is the one corresponding to the green region. We can see in

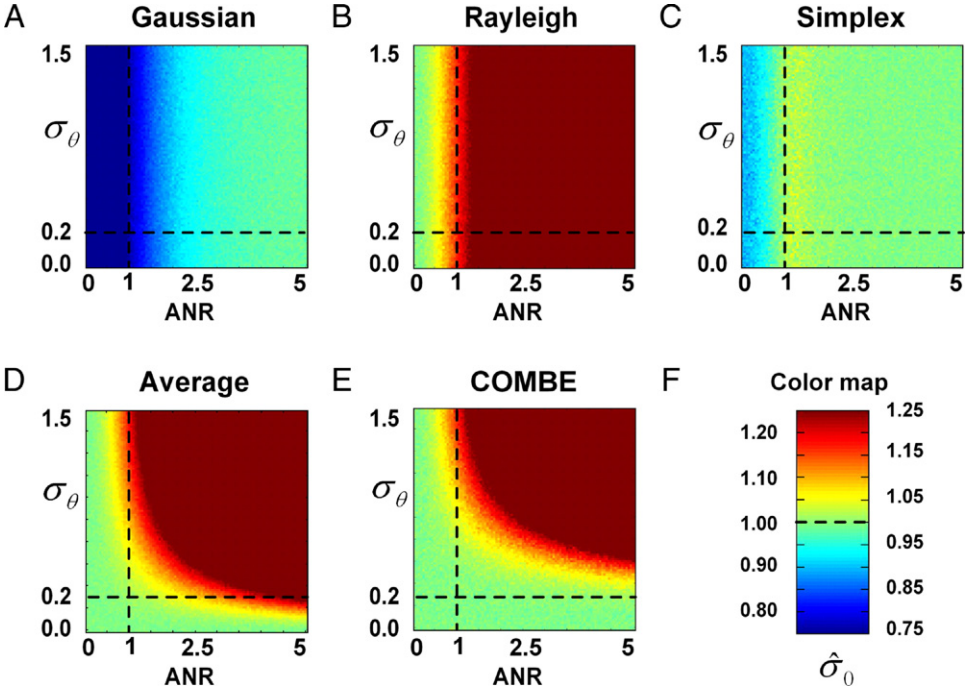

Fig. 1. Simulated estimation matrix maps for the five methods. The horizontal row of each matrix map corresponds to the ANR level from zero to five, while the vertical column corresponds to the standard deviation of the phase fluctuant from 0 to $\pi/2$. The estimated normalized standard deviation of thermal noise is color coded on the matrix map, especially with green corresponding to a theoretical value of one. (A) outlines the Gaussian method. (B) represents the Rayleigh method. (C) is for the Simplex method. (D) is for the Average method. (E) is for the COMBE method. (F) illustrates color coding. The horizontal dashed lines superposed on the matrix maps represent a special case $\sigma_\theta = 0.2$, while the ANR changes from zero to five. The vertical dashed lines superposed on the matrix maps represent another special case with ANR = 1, while σ_θ changes from 0 to $\pi/2$.

Fig. 1A that the Gaussian method drastically underestimates the noise standard deviation for a low ANR, regardless of the phase fluctuation standard deviation. In Fig. 1B, we can see that the Rayleigh method drastically overestimates the noise standard deviation for a large ANR, regardless of the phase fluctuation standard deviation. Moreover, the Simplex method underestimates the standard deviation of noise when the ANR is low, as shown in Fig. 1C. Nevertheless, in Fig. 1D and E, we can see that the Average and COMBE methods more accurately estimate the noise standard deviation for low/moderate ANR and phase fluctuation combinations. Furthermore, the COMBE method performs better over a larger combination of ANRs and phase fluctuations, as seen by its green region on the lower left part of Fig. 1E, than the Average method, with the green region on the lower left part of Fig. 1D.

The dependence of the thermal noise standard deviation estimate σ_0 on the ANR for each of the five noise-estimation methods is of interest. The 14th row above describes mean arrays for the estimated noise standard deviation σ_0 corresponding to a typical value (0.2 rad) of the phase fluctuation standard deviation, with an ANR varying from zero to five, as plotted in Fig. 2A, with the MSE depicted in Fig. 2B. As shown in Fig. 2A, when the ANR is close to zero, the Gaussian method (in blue) drastically underestimates the noise, as does the Simplex method in black (but to a lesser extent). The Rayleigh method (in green) correctly estimates the noise, while the estimated noise levels for the Average and COMBE methods (in yellow and red) are accurate and relatively unbiased. As the ANR increases, the Rayleigh method (in green) overestimates the noise and becomes more biased, while the Gaussian method yields a more unbiased estimate. The Average and COMBE methods yield relatively unbiased estimates for the ANRs until about two and four, respectively. The COMBE method with a smaller bias for all ANRs is considered. As seen in Fig. 2B, the COMBE method (in red) produced the lowest overall variability (i.e., the lowest MSEs for all ANRs considered among the five methods).

Also of interest within the simulation is the dependence of the thermal noise standard deviation estimate on the standard deviation of the phase fluctuation for each of the five noise-estimation methods. The 21st row above describes mean array surfaces for the estimated noise standard deviation σ_0 corresponding to an ANR of 1, with the phase fluctuation standard deviation varying from 0 to $\pi/2$ rad, as plotted in Fig. 2C. The MSEs of the estimation are plotted in Fig. 2D. As shown in Fig. 2C, since the ANR is fixed at 1, the Gaussian and Simplex methods (in blue and black) remarkably underestimate thermal noise, while the Rayleigh method (in green) significantly overestimates the noise. When the standard deviation of phase fluctuation is

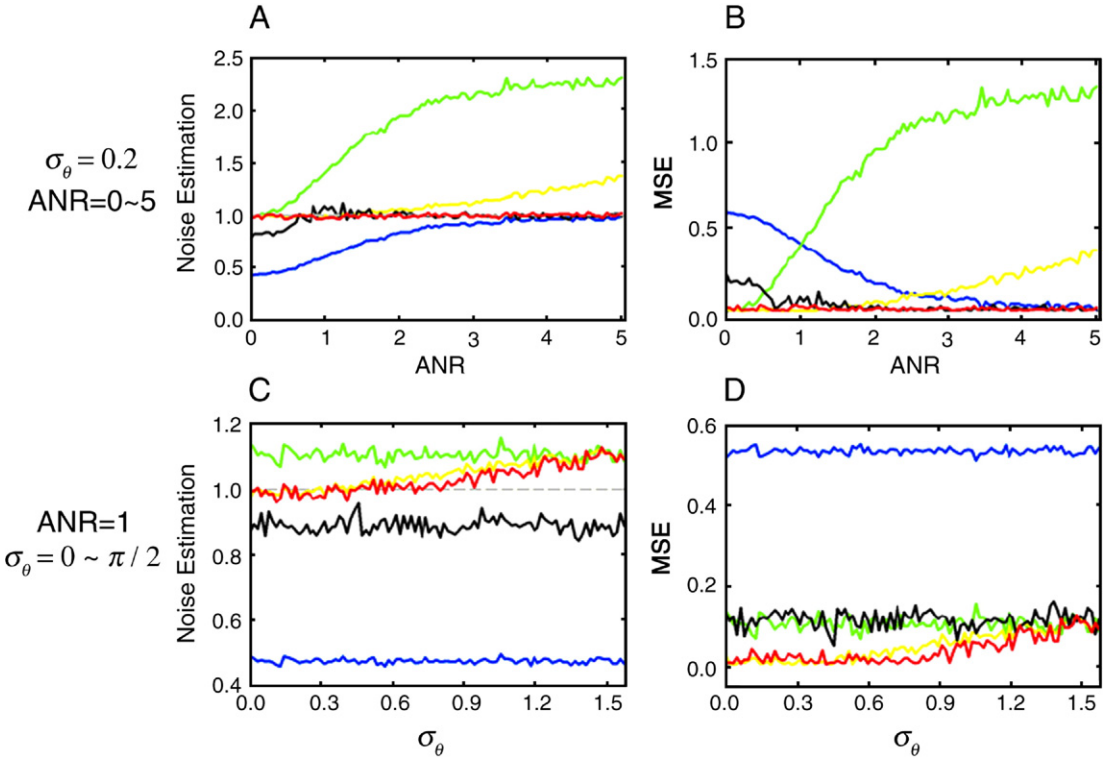

Fig. 2. Specific cases of the simulated estimations of thermal noise. The solid blue lines correspond to the Gaussian method; green lines are for the Rayleigh method; black lines represent the Simplex method; and yellow lines are for the Average method. The red lines are for the COMBE method. (A) presents the estimations when σ_θ is fixed at 0.2, while the ANR is scanned from zero to five, corresponding to the horizontal lines superposed on the matrix maps in Fig. 1A–E. (B) shows the MSE of the corresponding estimations. (C) presents the estimations when the ANR is fixed at 1, while the σ_θ is scanned from 0 to $\pi/2$, corresponding to the vertical dashed lines superposed on the matrix maps in Fig. 1A–E. (D) shows the MSE of the corresponding estimations.

small, both the Average and COMBE methods (in yellow and red) yield accurate and unbiased estimates. As the standard deviation of phase fluctuation increases, the Average method produces bias significantly more than the COMBE method. Overall, the latter consistently gives the most accurate unbiased estimation of the noise standard deviation when σ_0 varied from 0 to $\pi/2$, with an ANR of one. Fig. 2D shows that the COMBE method (in red) consistently produces the lowest overall variability in terms of the MSE for the estimation of the noise standard deviation among the five methods.

4. Experiments and results

All experimental fMRI data were obtained from a GE Signa 3.0-T scanner (GE Medical Systems, Milwaukee, WI) using a single-channel receiving coil. The experiment was conducted on two healthy young subjects using approved protocol from the Institutional Review Board and signed consent forms from the subjects. To demonstrate the performance of the five methods of noise estimation, a single-shot gradient-echo continued fMRI EPI sequence was employed with the following imaging parameters: T_R=1 s, T_E=30 ms, field of view =24 cm, single-slice covering, slice thickness=4 mm, matrix size=64×64, bandwidth=125 kHz. There were 220 repetitions. Each fMRI scan was conducted using a continued EPI sequence, with one axial slice across the upper part of the brain.

This continued EPI sequence comprises two parts. The first half scan used a 90° flip-angle radiofrequency (RF) pulse (i.e., 110 repetitions of RF-ON scan). In the second half, the RF pulse was nullified (i.e., 110 repetitions in RF-OFF scan). Therefore, the second half of the fMRI scan provided acquisition of pure thermal noise [4]. RF-ON time courses that were extracted from the first half (discarding the first and last five time points) were utilized to examine and compare the performances of the five estimation methods. RF-OFF time courses that were extracted from the second half (discarding the first and last five time points) were employed to estimate the underlying noise standard deviation. The estimated standard deviation of thermal noise for each method was defined as the average of the estimated standard deviations from all RF-OFF time courses in the image, which were obtained by the corresponding method. Since there were no artifacts existing in RF-OFF time courses, the estimation by the Average method was designated as benchmark values. Fig. 3 illustrates the data assignment for processing from the continued EPI sequence. All five methods were applied to RF-OFF time courses to compare their performances, and all estimation results were normalized by the corresponding benchmark value and presented in Table 1. For Subject 1, the Gaussian method yielded the normalized RF-OFF estimate of the thermal noise standard deviation for the whole image as 0.6679, 1.0195 for the Rayleigh method, 1.00001 for the COMBE method and 0.5451 for the Simplex method. For Subject 2, RF-OFF estimates for the thermal noise standard deviation gave 0.6859 for the Gaussian method, 1.0470 for the Rayleigh method, 1.0003 for the COMBE method and 0.5601 for the Simplex method. The COMBE method agrees with the Average method in estimating benchmark values.

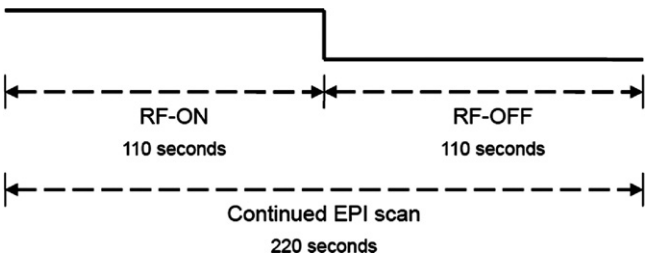

Fig. 3. Illustration of continued EPI data acquisition and corresponding RF-ON and RF-OFF datasets.

Table 1
The estimation of thermal noise (normalized on the benchmark value) in RF-OFF time courses

	Gaussian	Rayleigh	Simplex	Average	COMBE
Subject 1	0.6679	1.0195	0.5451	1	1.0000
Subject 2	0.6859	1.0470	0.5601	1	1.0003

To further evaluate the five estimation methods, the following steps were taken with RF-ON time courses. First, we segmented the brain region from the nonbrain region (background region) by using the plug-in "draw dataset" in the software package AFNI (Analysis of Functional NeuroImages) [22]. Then, each of the five methods was applied to every background voxel time course to obtain the voxelwise estimate of the artifact level, the standard deviation of phase fluctuation and the standard deviation of thermal noise. With the benchmark value (i.e., the underlying standard deviation of thermal noise), the ANR for each voxel time course was available. Then, all voxel time courses with a phase fluctuation standard deviation of <0.2 (determined by using Eq. (9)) and an ANR level of no more than 10 were pooled together as reliable voxel time course sets. For Subject 1, the number of background voxels (nonbrain region) was 2154 (i.e., 52.59% of whole-image voxels), while the number of reliable voxels reached 735 (i.e., 17.94% of whole-image voxels or 34.12% of background voxels). For Subject 2, the number of background voxels (nonbrain region) was 2318 (i.e., 56.59% of whole-image voxels), while the number of reliable voxels reached 539 (i.e., 13.15% of whole-image voxels or 25.03% of background voxels).

For each subject, within reliable voxels, the estimated noise from each method was aggregated into ANR sets according to their corresponding ANRs. The aggregation of the estimation was based on rounding the ANRs to their nearest integers (e.g., a voxel time course with ANR=3.7 was aggregated to a set with ANR=4, while ANR=0.4 was included in the set with ANR=0). Within each ANR set, the mean value and MSE of the estimations were obtained. All

mean values of each ANR set were divided by the benchmark values to obtain normalized estimation results. Thus, the dependency estimations of the ANR from the experiment data were at hand, which are also illustrated in Fig. 4.

The normalized estimation results are shown in Fig. 4 and listed in Table 2. As shown in Fig. 4, the five estimations repeat the pattern that was shown in Fig. 2A: the Gaussian method underestimates when the ANR is small; the Rayleigh method overestimates over all ANR levels; the Simplex method underestimates and introduces significant large variabilities (i.e., the MSEs); the Average method shows significant bias when the ANR increases; and the COMBE method yields much less bias through all ANRs. Hence, it provides the most optimal estimation among the five methods. The normalized estimation results are also provided in Table 2. If we define ±10% as an acceptable range (superposed as gray bars on Fig. 4A) for the estimation of the standard deviation of thermal noise, then as seen in Fig. 4A for Subject 1, the Gaussian method (in blue) is good from ANR=2 to ANR=10. The Rayleigh method (in green) has no good range. The Simplex method (in black) is reasonable from ANR=7 to ANR=10. The Average method (in yellow) is acceptable from ANR=0 to ANR=8. Finally, the COMBE method (in red) is superior to the other methods through all ANR sets (0–10). The scan for Subject 2 presented more significant artifacts and, therefore, decreased acceptable regions for the estimation of all five methods. Still, the COMBE method outperforms all the others. As seen in Fig. 4C for Subject 2, the acceptable range (i.e., ±10% error; superposed as gray bars on Fig. 4C)

Table 2
The estimation of thermal noise (normalized mean value) on integer ANR sets from reliable background voxel time courses

ANR	Gaussian	Rayleigh	Simplex	Average	COMBE
(A) Estimation for Subject 1					
0	0.7318	1.1171	0.6605	0.9139	0.9072
1	0.8763	1.3375	0.7519	0.9643	0.9458
2	0.9622	1.4687	0.8215	1.0196	0.9849
3	0.9769	1.4911	0.7976	1.0224	0.9810
4	1.0019	1.5293	0.7854	1.0427	0.9965
5	1.0332	1.5771	0.9139	1.0716	1.0118
6	1.0109	1.5430	0.8815	1.0637	1.0057
7	1.0182	1.5542	0.9142	1.0853	1.0228
8	1.0273	1.5681	0.9061	1.0834	1.0262
9	1.0452	1.5954	0.9849	1.1457	1.0332
10	1.0290	1.5706	0.9088	1.1119	1.0231
(B) Estimation for Subject 2					
0	0.7601	1.1602	0.6728	0.9522	0.9464
1	0.8870	1.3538	0.6941	0.9948	0.9765
2	0.9872	1.5069	0.8648	1.0421	1.0064
3	1.0387	1.5854	0.9048	1.0745	1.0235
4	1.0439	1.5934	0.9642	1.1031	1.0366
5	1.0923	1.6673	0.9615	1.1604	1.0833
6	1.1207	1.7107	1.0054	1.2458	1.1595
7	1.0440	1.5936	0.7610	1.1247	1.0546
8	1.1046	1.6860	0.8843	1.2145	1.1067
9	1.1757	1.7946	0.9680	1.3057	1.1834
10	1.1224	1.7133	0.9490	1.2670	1.1381

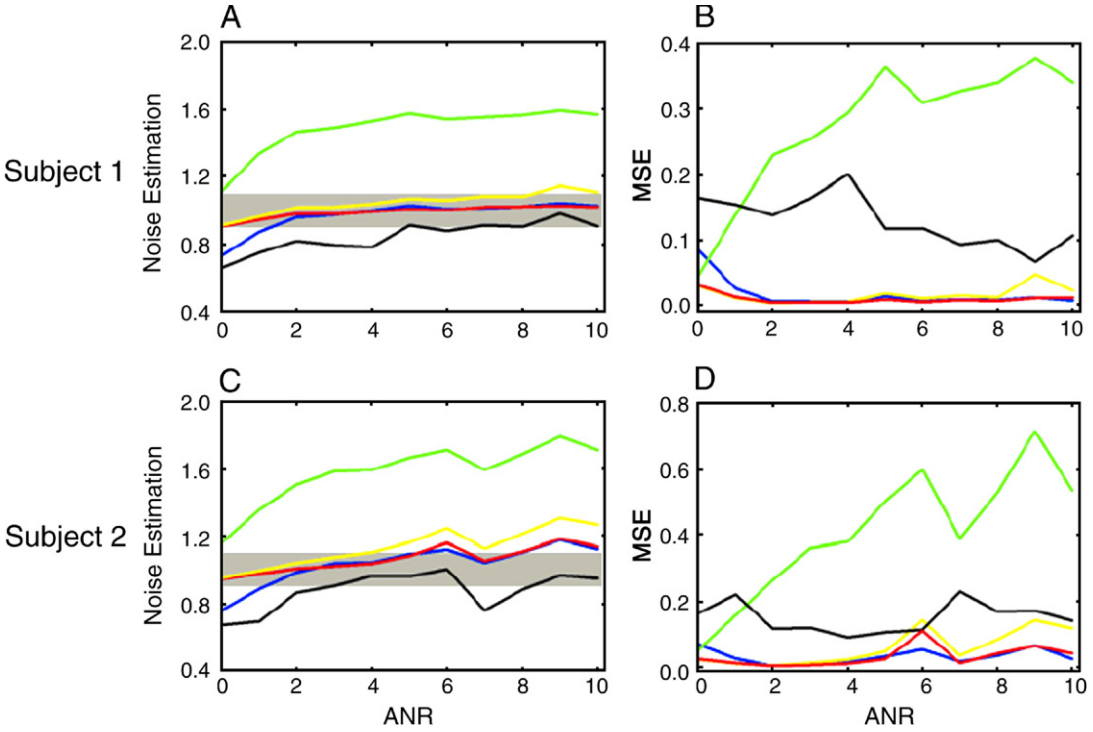

Fig. 4. Estimation of thermal noise on experimental results. The solid blue lines correspond to the Gaussian method; green lines are for the Rayleigh method; black lines are for the Simplex method; red lines are for the COMBE method; while yellow lines are for the Average method. (A) presents the estimations for Subject 1, scanning reliable background voxels with ANR sets from 0 to 10. (B) shows the MSEs of the corresponding estimations. (C) presents the estimations for Subject 2. (D) shows the MSEs of the corresponding estimations. The superposed gray horizontal bars in (A) and (C) indicate the defined acceptable regions within ±10% of errors for the estimation of the standard deviation of thermal noise.

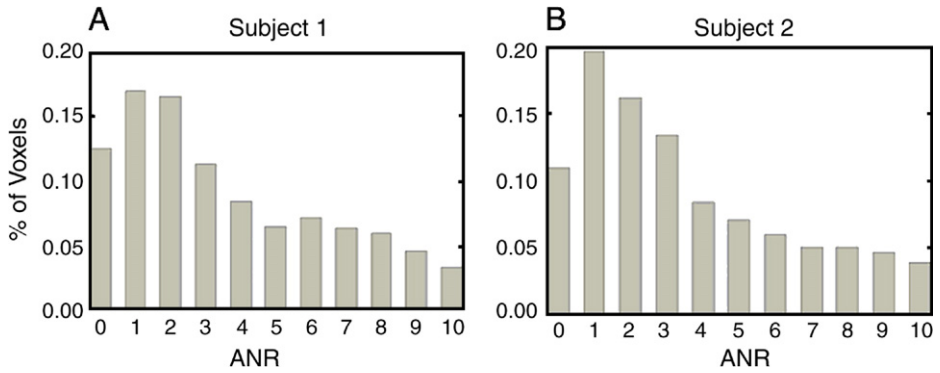

Fig. 5. Histogram of reliable voxel sets for the ANR level. (A) represents Subject 1. (B) pertains to Subject 2. The vertical axis is the ratio of the number of voxels in each ANR set to the number of all reliable voxels for each subject.

for the Gaussian method (in blue) is ANR=2–5, no good range for the Rayleigh method (in green), ANR=3–6 for the Simplex method (in black), ANR=0–3 for the Average method (in yellow), while the COMBE method (in red) is superior to the other methods with the longest range, ANR=0–5. The COMBE method also produces the lowest MSE among all five methods for both subjects, as shown in Fig. 4C and D. Histograms for the number of reliable voxels for the subjects in terms of ANR levels are presented in Fig. 5.

5. Discussion

For comparison, the five methods (Gaussian, Rayleigh, Simplex, Average and COMBE) were employed to estimate thermal noise in fMRI datasets when a significant source of artifact noise was considered. With theoretical simulation and experimental fMRI datasets, the COMBE method, which we have described, provides the best noise estimation among the five. The Gaussian and Rayleigh methods cannot provide accurate and reliable estimates in the presence of artifacts. It is very difficult to select an artifact-free region in magnitude images acquired by fast-imaging pulse sequences, such as EPI and spiral. Thus, a method that can tolerate the presence of artifacts is necessary. The Simplex method is very time consuming, is easily trapped into local minimum and cannot ensure accurate convergence for a considerable number of voxel time courses. The Average method can provide accurate thermal noise estimation, if phase fluctuations are small. However, our experimental results indicate that phase fluctuations clearly exist, resulting in significant overestimation by the Average method. The newly proposed COMBE method not only employs the complex-valued dataset (thereby avoiding the disadvantages of magnitude images) but also identifies voxel sets based on artifact levels and phase fluctuations with its step-by-step procedures.

It is important to clarify several key issues. First, the benchmark of the underlying standard deviation of thermal noise is determined using the estimation of Average method from RF-OFF time courses, which is extracted from the same continued EPI acquisition. In the past, thermal noise was determined by a separate scan with no RF pulse [4]. The continued scan further eliminates uncontrollable factors between the setups of the scans to ensure that the statistical characteristics of thermal noise will not be changed. Although phantom studies have confirmed this assumption (data not shown here), the complexity involving human subjects can undermine the validation of the benchmark value by some unforeseeable causes. This issue needs further investigation.

There are several noticeable discrepancies between theoretical simulation and experimental results. First, when the ANR increases, the COMBE method also begins to overestimate thermal noise for the experiment data even with a restricted standard deviation of phase fluctuation ($\sigma_\theta<0.2$). This is primarily because the fluctuation of the artifacts in the time domain $\gamma\Delta S(t)$, which was described in the Theory section, begins to play an observable role. None of the methods can avoid the effect of this fluctuation. The existence of significant artifact fluctuation in large ANR situations is confirmed by the overestimation of the Gaussian method (in blue). This indicates that, in addition to thermal noise, there are other temporal magnitude fluctuations. It is interesting to note that even with the fluctuation of artifacts in play, the COMBE estimation performs at least as well as the Gaussian method. This demonstrates that both methods yield the combined variance of thermal noise and artifact fluctuation, which are optimal under the circumstance. As stated in the Theory section, the artifact proportionality γ determines what degree of artifact fluctuations will be ghosted into background voxel time courses. The ghosted fluctuation $\gamma\Delta S(t)$ cannot be neglected when compared to the standard deviation of thermal noise σ_0. Therefore, the estimation will show some bias. In reality, those voxels with high ANR levels, which contain non-negligible artifact fluctuations, can be excluded from the estimation to avoid contamination by artifact fluctuation. Second, the Rayleigh method significantly overestimates thermal noise even with the set with ANR=0, although, theoretically, it should give the correct answer. There are the following possible causes: The set with ANR=0 may include a significant portion of nonzero ANR voxel time

courses because the set is composed of voxel time courses with the ANR from 0 to 0.5; or the benchmark value possibly underestimates thermal noise for RF-ON time courses; thermal noise may deviate slightly from the Gaussian distribution of real and imaginary channel data from experimental data. Third, it is possible that the Simplex method significantly underperforms in experimental data as compared to the simulations. We have come up with two explanations. Perhaps, experimental data were more complicated, imposing challenges on the Simplex method to reach the global minimum. Actually, there were a significant number of reliable voxel time courses that were rejected by the MATLAB program due to divergence. The second premise is that the possible non-Gaussian nature of thermal noise distribution, which undermines the foundation of the Simplex method, is based on the Rician distribution of voxel time courses.

Although thermal noise has been viewed as independently Gaussian distributed in both I channel (real-part data) and Q channel (imaginary-part data), this rule could be challenged. We investigated this in experimental data by computing the kurtosis for RF-OFF time courses. Theoretically, the kurtosis for a Gaussian-distributed random variable should be 3. In our data, they were 3.0818 ± 0.5146 for I channel (real data) and 3.0701 ± 0.5019 for Q channel (imaginary data) for Subject 1; and 3.0718 ± 0.5048 for I channel (real data) and 3.0628 ± 0.4977 for Q channel (imaginary data) for Subject 2. In addition, we conducted a simulation with matched datasets (4096 Gaussian-distributed voxel time courses with 100 time points) in MATLAB, and the simulated kurtosis was 3.0008 ± 0.4938. The difference is not statistically significant. However, the difference between mean values, which usually will be taken as the ultimate estimation result, is noticeable. In addition, in RF-OFF time courses, the Rayleigh method still overestimates thermal noise by nearly 2% for Subject 1 and by 5% for Subject 2. Although the discrepancy of statistical characteristics can be neglected in most circumstances, it does diminish the validation of the Rayleigh method and the Simplex method.

Even though real-noise data show a slight deviation from Gaussian distribution, we still recommend disregarding this issue in conventional linear reconstructed fMRI data. Still, recent emerging nonlinear reconstruction schema presented non-Gaussian-distributed thermal noise [23–25] and rendered the magnitude image incapable of being modeled as a Rician distribution [26]. This invalidated both the Rayleigh method and the Simplex method. The COMBE method does not assume a specific statistical distribution for thermal noise. Therefore, it can adapt to new reconstruction schemes that do not produce Gaussian noise, as long as they retain the independence of the I and Q channels and remain stationary of thermal noise in the time domain. The Average method in Eq. (14) does not have to rely on the premise of the Gaussian distribution of thermal noise. However, ML approaches cannot be used to reach the Average method.

There are two goals for noise estimation. First, the emphasis is on overall noise estimation, which assumes that the same noise distribution in the whole image remains identical over both the spatial domain and the time domain. Therefore, by collecting a sufficient number of voxels, the COMBE method can yield an optimal estimate. Parallel imaging such as SENSE [27] yields noise that is not uniform over the image. The proposed COMBE method can be implemented for individual voxel noise estimation. Because of its broad adaptive capability, it can be applied to more types of voxels with different properties compared to other methods listed in this study.

In current high-field studies, the SNR is generally sufficient for most applications, which makes noise estimation a less important topic in regular BOLD activation studies. However, there are still two fields requiring accurate noise estimation. One is functional connectivity study, which focuses on one sort of physiologic noise (spontaneous low-frequency fluctuation). The intensity of the fluctuation is comparable to the standard deviation of thermal noise [8,28,29]. In addition, the evaluation of the development of novel reconstruction algorithms requires accurate estimation. The proposed COMBE method not only provides an accurate estimation of thermal noise but also gives the measurement of the artifacts (and the phase fluctuation of the artifacts), which is an important gauge for sequence design and reconstruction development [30,31] (e.g., a better reconstruction schema yields less presence of artifacts).

In conclusion, in the abovementioned fMRI studies, the COMBE method can be employed to estimate the thermal noise level in the presence of artifacts and phase fluctuation. In addition, it provides an optimal and reliable estimation by adapting to voxel time courses with a wider variety of characteristics than other methods. Further, it requires fewer assumptions, specifically the statistical distribution of thermal noise required by conventional methods. Thus, it is suitable for use in more fMRI studies, especially functional connectivity studies and reconstruction optimization.

Acknowledgments

This study was supported, in part, by the Extendicare Foundation, the Dana Foundation and National Institutes of Health research grants AG20279 and RR00058. We thank Ms. Carrie O'Connor, MA, for editorial assistance.

References

[1] Yacoub E, Duong TQ, Van De Moortele P, Lindquist M, Adriany G, Kim SG, et al. Spin-echo fMRI in humans using high spatial resolutions and high magnetic fields. Magn Reson Med 2003; 49:655–64.

[2] Preston A, Thomason M, Ochsner K, Cooper J, Glover GH. Comparison of spiral-in/out and spiral-out BOLD fMRI at 1.5 and 3 T. Neuroimage 2004;21:291–301.

[3] Wang FN, Huang TY, Lin FH, Chuang TC, Chen NK, Chung HW, et al. PROPELLER EPI: an MRI technique suitable for diffusion tensor imaging at high field strength with reduced geometric distortions. Magn Reson Med 2005;54:1232–40.
[4] Kellman P, McVeigh E. Image reconstruction in SNR units: a general method for SNR measurement. Magn Reson Med 2005;54:1439–47.
[5] Henkelman R. Measurement of signal intensities in the presence of noise in MR images. Med Phys 1985;12:232–3.
[6] Edelstein W, Bottomley P, Pfeifer L. A signal-to-noise calibration procedure for NMR imaging system. Med Phys 1984;11: 180–5.
[7] Gudbjartsson H, Patz S. The Rician distribution of noisy MRI data. Magn Reson Med 1995;34:910–4.
[8] Krüger G, Glover GH. Physiological noise in oxygenation-sensitive magnetic resonance imaging. Magn Reson Med 2001; 46:631–7.
[9] Buonocore M, Gao L. Ghost artifact reduction for echo planar imaging using image phase correction. Magn Reson Med 1997; 38:448–53.
[10] Glover G, Lai S. Self-navigated spiral fMRI: interleaved versus single shot. Magn Reson Med 1998;39:361–8.
[11] Dietrich O, Heiland S, Sartor K. Noise correction for the exact determination of apparent diffusion coefficients at low SNR. Magn Reson Med 2001;45:448–53.
[12] Sijbers J, den Dekker A. Maximum likelihood estimation of signal amplitude and noise variance from MR data. Magn Reson Med 2004;51:586–94.
[13] de Zwart J, Ledden P, van Gelderen P, Bodurka J, Chu R, Duyn J. Signal-to-noise ratio and parallel imaging performance of a 16-channel receive-only brain coil array at 3.0 Tesla. Magn Reson Med 2004;51:22–6.
[14] Rowe DB. Parameter estimation in the magnitude-only and complex-valued fMRI data models. Neuroimage 2005;25:1124–32.
[15] Sijbers J, den Dekker A, Verhoye M, Audekerke J, Van Dyck D. Estimation of noise from magnitude MR images. Magn Reson Imaging 1998;16:87–90.
[16] Noll D, Nishimura D, Macovski A. Homodyne detection in magnetic resonance imaging. IEEE Trans Med Imaging 1991;10:154–63.
[17] Haacke M, Brown R, Thompson M, Venkatesan R. Magnetic resonance imaging: physical principles and sequence design. New York: John Wiley and Sons; 1999. p. 331–80.
[18] Rowe DB, Logan BR. A complex way to compute fMRI activation. Neuroimage 2004;23:1078–92.
[19] Bain L, Engelhardt M. Introduction to probability and mathematical statistics. 2nd ed. Boston (MA): Duxbury Press; 2000.
[20] Wink A, Roerdink J. Denoising functional MR images: a comparison of wavelet denoising and Gaussian smoothing. IEEE Trans Med Imaging 2004;23:374–87.
[21] Lagarias J, Reeds J, Wright M, Wright P. Convergence properties of the Nelder–Mead Simplex method in low dimensions. SIAM J Optim 1998;9:112–47.
[22] Cox R. AFNI: software for analysis and visualization of functional magnetic resonance neuroimages. Comput Biomed Res 1996;29: 162–73.
[23] Singh R, Deshpande V, Haacke M, Shea S, Xu Y, McCarthy R, et al. Coronary artery imaging using three-dimensional breath-hold steady-state free precession with two-dimensional iterative partial Fourier reconstruction. J Magn Reson Imaging 2004;19;645–649.
[24] Peng H, Sabati M, Lauzon M, Frayne R. Reconstruction of MR images from sparsely sampled 3-D *K*-space data. Proc Intl Soc Magn Reson Med 2005;13:2301.
[25] Chang T, He L, Fang T. MR image reconstruction from sparse radial samples using Bregman iteration. Proc Intl Soc Magn Reson Med 2006;14:696.
[26] Sabati M, Peng H, Frayne R. Noise characteristics in POCS (Projection Onto Convex Sets)-reconstructed MR images. Proc Intl Soc Magn Reson Med 2006;14:2940.
[27] Pruessmann K, Weiger M, Scheidegger M, Boesiger P. SENSE: sensitivity encoding for fast MRI. Magn Reson Med 1999;42: 1439–47.
[28] Xu Y, Xu G, Wu G, Li S. Group phase delay affects the measurement of functional synchrony. Proc Intl Soc Magn Reson Med 2004;12:498.
[29] Xu G, Xu Y, Wu G, Antuono P, Hammeke T, Li SJ. Task-modulation of functional synchrony between spontaneous low-frequency oscillations in the human brain detected by fMRI. Magn Reson Med 2006;56:41–50.
[30] Nunes R, Jezzard P, Behrens T, Clare S. Self-navigated multishot echo-planar pulse sequence for high-resolution diffusion-weighted imaging. Magn Reson Med 2005;53:1474–8.
[31] Robson M, Porter D. Reconstruction as a source of artifact in non-gated single-shot diffusion-weighted EPI. Magn Reson Imaging 2005;23:899–905.